same geometrical shape correspond to the same compound nuclei. It seems clear that a relationship exists between the threshold displacements and angular momentum of the compound nuclei, but again it is not possible to distinguish between a linear or a quadratic form on the basis of goodness-of-fit. It is worth noting, however, that in 3(b) the threshold displacement approaches zero as $\langle J^2 \rangle$ goes to zero, whereas in 3(a) the displacement approaches zero at an appreciable value of $\langle J \rangle$. The error bars indicated in Fig. 3 correspond to ± 1 MeV, which is surely an underestimate of the uncertainty in the extrapolation procedure, and it may be somewhat fortuitous that the data appear to correlate so strongly. (As a point of interest, if we had neglected any contributions of target and projectile spins in the angular momentum averaging, the resulting correlations would infer better agreement with a linear dependence on angular momentum as compared to a quadratic one.)

Alexander and Simonoff have extensively studied excitation functions for neutron-emitting reactions from Dy compound nuclei.[4] Our experiments are very similar in character to theirs, one notable difference being the projectiles used to induce the various reactions. Alexander and Simonoff employed beams ranging from C^{12} to Ne^{22}, whereas we have used the lighter ions He^4 to N^{14}. It was of interest to determine whether the excitation functions for our (HI,xn) reactions would peak at the same values of $(E_{c.m.}+Q)/x$ as found for Dy systems, or whether there was a systematic dependence on the details of energy (and angular momentum) deposition. Our result that $(E_{c.m.}+Q)/x=4.8$–6.3 MeV for Sm systems is essentially the same as the values 5.0–6.5 MeV for Dy compound nuclei. Alexander and Simonoff[4] have carried out a considerably more detailed analysis of their excitation-function data than we have presented here. They have derived average excitation energies minus neutron binding energies for the reactions (equivalent to $E_{c.m.}+Q$ appropriately averaged over a full excitation function) and found a strong correlation with angular momentum. Our observations in Figs. 2 and 3 are closely related to their result. These phenomena are almost certainly manifestations of gamma-ray competition with neutron emission,[6] a subject which will undoubtedly be intensively studied in the future, and with which we shall not attempt to deal at this time.

PHYSICAL REVIEW VOLUME 143, NUMBER 3 MARCH 1966

Scattering of 150- and 300-MeV Positrons and Electrons from Bismuth

A. BROWMAN,* B. GROSSETÊTE, AND D. YOUNT†
Ecole Normale Supérieure, Laboratoire de l'Accélérateur Linéaire, Orsay, France
(Received 1 October 1965)

Positrons and electrons from the Orsay linear accelerator were scattered from bismuth at 6°, 10°, 15°, and 20° at 300 MeV, and at angles having similar momentum transfers at 150 MeV. In addition to electron-positron ratios, relative and absolute cross sections were measured and are given here for the present experiment as well as for the high- and the low-resolution experiments reported earlier. The latter data extend to 45° at 300 MeV ($q^2 \approx 1.4$ F^{-2}). The combined data from the three experiments are internally consistent and are in general agreement with the partial-wave predictions based on earlier electron scattering results. However, the electron-positron ratio in the neighborhood of the 6°, 300-MeV point disagrees by 2.2 standard deviations with the partial-wave predictions and also with the value for the ratio obtained at the corresponding 150-MeV point when the latter is scaled to 300 MeV by means of a "model-independent" scaling law. The present data thus confirm the discrepancy noted earlier in which the results of Goldemberg, Pine, and Yount at 5° and 300 MeV disagreed with the partial-wave predictions and with the scaled results of Miller and Robinson taken at energies below 170 MeV.

I. INTRODUCTION

PREVIOUS experiments[1,2] in which high-energy positrons and electrons have been scattered from medium and high-Z nuclei at equal incident energies and scattering angles have yielded results in "remarkably close" agreement with partial-wave calculations[3] based on *static* charge distributions extracted from earlier electron scattering data.[4] In spite of the good general agreement, however, several of the points in Ref. 2 disagree with the partial-wave predictions and also with the results of Ref. 1 when the latter are scaled to the higher energies of Ref. 2 by a small angle model-independent scaling law based upon the second Born approximation.[5]

The present experiment was motivated primarily by the possibility that both of the previous experiments were correct and the scaling law as well as the partial-

* Present address: Cornell University, Ithaca, New York.
† Now at Stanford Linear Accelerator Center, Stanford, California.

[1] R. C. Miller and C. S. Robinson, Ann. Phys. (N. Y.) **2**, 129 (1957).
[2] J. Goldemberg, J. Pine, and D. Yount, Phys. Rev. **132**, 406 (1963).
[3] R. Herman, B. C. Clark, and D. G. Ravenhall, Phys. Rev. **132**, 414 (1963).
[4] B. Hahn, D. G. Ravenhall, and R. Hofstadter, Phys. Rev. **101**, 1131 (1956).
[5] S. D. Drell and R. H. Pratt, Phys. Rev. **125**, 1394 (1962).

wave calculations are not valid for the energy and angles studied. Conceivably, the partial-wave calculations might succeed in fitting either the experimental electron-positron "ratios" or the "relative cross sections" for positrons or for electrons but be inconsistent with the combined data. Although a failure of the scaling law, and thus of the second Born approximation, would not be particularly surprising in the case of a high Z element such as bismuth (even at the low momentum transfers of the small-angle points), a failure of the partial-wave calculations would seem to have more serious consequences. Such a result could, for example, be due to some energy-dependent dynamical effects which are not included in either the scaling law or in the partial-wave calculations.[3]

If the partial-wave calculations were confirmed, one might conclude that there is no longer any reason to continue the positron measurements. The view has, for example, been expressed "that the electron-positron difference may be regarded as an essentially kinematic effect, probably quite insensitive to nuclear dimensions."[6] We wish to emphasize, however, that the use of positrons with electrons is an experimental question. The sign of the incident particle is simply one of the parameters which the experimenter can vary. He may choose to vary this parameter even if the variation of other parameters, such as the incident energy and the scattering angle, gives equivalent information. This choice can be justified in practice by the fact the ratio measurements have thus far been made with greater precision than the relative cross-section measurements, even when both were obtained in the same experiment.[2,7] For high-Z elements where the effects are large, the greater precision of the ratio measurements implies a greater sensitivity to certain features of the nuclear charge distributions. The high sensitivity of the positron-electron ratios has been demonstrated in the case of at least one low-Z element, namely the proton, where small, possibly mesodynamical effects have been found.[7–9]

As a result of the present work and a re-evaluation of the two experiments reported in Ref. 2, we now believe that *some* of the observed discrepancies were due in part to a strong enhancement of the multiple scattering in the previous low-resolution experiment. This enhancement, for which a correction can be made, resulted from the three beam monitors installed upstream from the target to permit data to be taken at very small angles. In all of the other positron-scattering experiments carried out by the Stanford group, including the high-resolution experiment of Ref. 2, the beam monitors were downstream from the target. In the present experiment, the beam monitors were again upstream from the target, but we have greatly reduced the multiple-scattering problem by using very thin monitors and a target of roughly half the thickness of that previously.

We have retaken the 5°, 10°, 15°, and 20° points of the low-resolution bismuth experiment at 300 MeV. In addition, we have taken the four corresponding points at 150 MeV having the same momentum transfer. For each of the eight positron and eight electron measurements, we have obtained absolute and relative cross sections as well as the electron-positron ratios, Finally, we are publishing for the first time the relative and absolute cross-section measurements obtained during the course of the previous high- and low-resolution experiments on cobalt and bismuth. Our present confidence in these data results from the improved internal consistency achieved when differences in multiple scattering and in the resulting angular resolution are properly taken into account.

II. APPARATUS

The experimental set-up as it appeared from the side is shown in Fig. 1. Momentum-analyzed positron[10,11] and electron beams from the Orsay Linear Accelerator passed through thin ionization chamber monitors and were incident on a bismuth target located at the center of rotation of the double-focusing, zero-dispersion spectrometer.[12] The recoil positrons or electrons were momentum analyzed in the spectrometer and were then detected by scintillation counters. Another ion chamber placed just in front of the counters was used to measure the beam direction and to remeasure the incident momentum and momentum distribution. The target and beam monitors were enclosed in a helium-filled sack to reduce multiple scattering and empty target background.

The three-magnet system used to momentum-analyze the incident beams[12,13] has been calibrated by a floating-wire measurement[14] believed to be accurate to several parts in 10^3. The field in the first analyzing magnet was monitored during the runs with an NMR probe. On reversals between electrons and positrons, the NMR and shunt readings agreed within $\pm 0.2\%$. The momentum slits were set at $\Delta p/p = \pm 1\%$, and an 11 mm$\times$11 mm collimator was used.

The beam monitors consisted of three thin-walled, hydrogen-filled ion chambers having sensitive volumes defined by parallel aluminum plates oriented perpendicular to the beam direction. Two of these were used to monitor the beam intensity while the third, a split-plate

[6] A. Baker, Phys. Rev. **134**, B240 (1964).
[7] D. Yount and J. Pine, Phys. Rev. **128**, 1842 (1962).
[8] A. Browman, F. Liu, and C. Schaerf, Phys. Rev. Letters **12**, 183 (1964).
[9] A. Browman, F. Liu, and C. Schaerf, Phys. Rev. **139**, B1079 (1965).
[10] T. L. Aggson and L. Burnod, Orsay Linear Electron Accelerator Technical Report No. LAL-27, 1962 (unpublished).
[11] R. Hirel, L. Burnod, and G. Delouya, Orsay Linear Electron Accelerator Technical Report No. LAL-28, 1962 (unpublished).
[12] B. Milman, L'Onde Elec. **42**, 310 (1962).
[13] B. Milman, Nucl. Instr. Methods **20**, 13 (1963).
[14] C. Bazin, J. Dupin, and N. K. Loï, Orsay Linear Electron Accelerator Internal Report No. RI-65-1, 1965 (unpublished). See also P. Bounin and B. Milman, Rev. Sci. Instr. **34**, 1448 (1963).

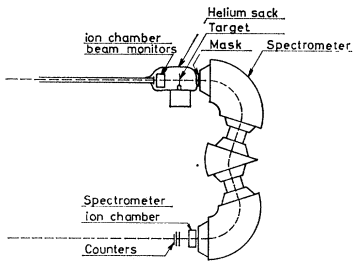

FIG. 1. Side view of the experimental setup. Momentum-analyzed positrons or electrons passed through the thin ionization chamber monitors and were incident on a bismuth target at the center of the spectrometer. The recoil positrons or electrons were momentum analyzed by the spectrometer and were detected by scintillation counters. An ionization chamber was also used to detect particles transmitted by the spectrometer during certain tests described in the text.

chamber similar to that described in Ref. 7, was used as a beam position indicator. To minimize the number of entrance and exit windows, the three monitors were enclosed in a single gas-tight container through which hydrogen was flowed at ambient temperature and pressure. Temperature and pressure corrections of order 1% were made to the ion-chamber efficiencies. The two ion chambers which monitored beam intensity had different thicknesses and thus different saturation characteristics. This helped to insure that at all times the monitors were being used at beam-current densities well below the saturation level of either chamber. The beams were centered at the target to about ± 1 mm with the aid of the beam position indicator. Beam sizes and positions were checked with a fluorescent screen with electrons and with polaroid film placed directly in the beam for positrons. The beams were rectangular in shape, about 1 cm wide and 1.5 cm high at the target.

The "1 BeV" Orsay Faraday cup[15] was used to calibrate the ion chamber beam monitors. Its efficiency was taken to be 1.00 ± 0.01 for both positrons and electrons. We have not, however, tested this Faraday cup independently to determine its absolute efficiency or its relative efficiency for positrons and electrons. For the electron-positron ratios we are dependent upon previous tests described in Ref. 7, which indicate that the ionization of hydrogen, and thus the efficiency of the ion chamber beam monitors, is the same for positrons and electrons to $(0.00\pm0.15)\%$ at energies and under conditions comparable with those of interest here. Intercalibrations of the ion chambers and the Orsay Faraday cup indicate that the Faraday cup efficiency for positrons differs from its efficiency for electrons by $(0.4\pm0.2)\%$.[16] We have used other data reported in Refs. 7 and 16 to estimate a 0.1% correction in the ion chamber efficiency which is applicable in comparing relative cross sections measured at 150 and 300 MeV.

The bismuth target was 5 cm$\times$5 cm with a thickness of 0.119 ± 0.001 g/cm^2 (about 0.018 radiation lengths). The target thickness was uniform to within 0.5% over the center 2.7 cm square region, and target impurities were negligible.

Two spectrometer entrance masks, having effective diameters of (5.00 ± 0.02) and (20.0 ± 0.2) mm, respectively, were used in order to achieve convenient counting rates in spite of the rapidly varying cross sections. The masks defined the solid angle and geometrical angular resolution and insured a uniform spectrometer response over the incident-beam distribution at the target. The smaller mask, made of 10-mm-thick tungsten, was tapered in such a way that for the entire target region the solid angle was defined by the mask face nearest the target. Mask penetration of about 1% was measured by adding a tapered conical plug at the entrance face of the mask. The plug had a maximum diameter just equal to the minimum mask diameter and continued the mask taper through the same thickness of tungsten as the mask proper. Since the large mask, made of 23.5-mm-thick lead, had a diameter greater than the beam diameter at the target, no taper was necessary; and the solid angle was defined by the mask face farthest from the target. The mask penetration in this case was expected to be negligible. The small mask was used at 6° and 10° at 300 MeV while the large mask was used at all other points. The masks were intercalibrated at the 15°, 300-MeV electron point.

A pointer attached to the spectrometer indicated the nominal scattering angle on a scale from 0° to 360° inscribed around the base of the spectrometer. The scale was divided into units of 0.05° and could be read by means of closed circuit television to an accuracy of $\pm0.01°$. The direction of the beam in the scattering plane was measured using the beam ion chambers and a third ion chamber located near the exit window of the spectrometer. The spectrometer without masks was set at the incident momentum, and the ratio of the ion-chamber currents was obtained as a function of angle near 0°. This also determined the "natural" angular acceptance of the spectrometer and the beam-spot distribution in the scattering plane. The beam directions measured in this way were accurate to about $\pm0.05°$, and the results were consistent with counting rates observed on the left and on the right of the beam line with the masks in place. While the effective beam angles sometimes differed from 0° by a few tenths of a degree, they were *stable* for a given beam to $\pm0.01°$. Thus, by taking data at each point with the spectrometer on the left and on the right of the beam line, we were able to reduce the angle errors by an order of magnitude and evaluate them. Nearly symmetrical angles were chosen in order to avoid the angle correction which must be made to the average of the left and right measurements when large left-right asymmetries are observed. Except for the prior measurement of the beam direction, the angle-cycling used here is equivalent to that described in Refs. 2 and 7.

A high-precision shunt, calibrated with a floating wire

[15] D. Isabelle, L'Onde Elec. 42, 354 (1962).
[16] A. Browman, B. Grossetête, and D. Yount (unpublished).

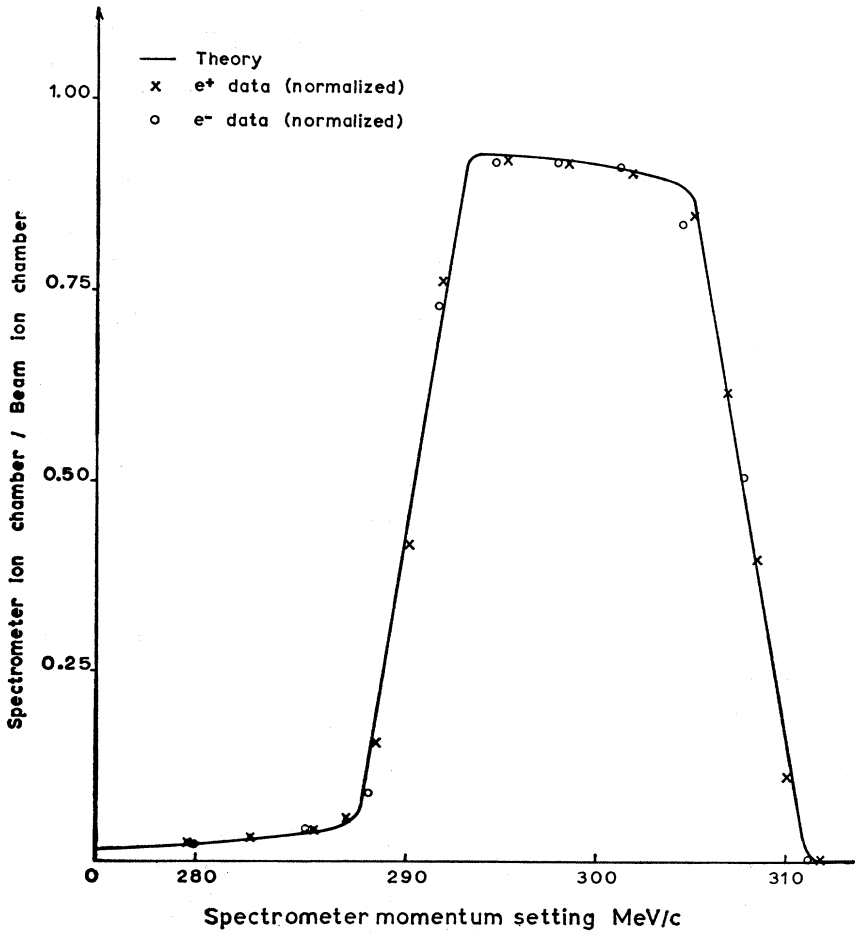

FIG. 2. Spectrum studies for positrons and electrons at 300 MeV. The solid curve is the predicted spectrum for a trapezoidal incident energy distribution $\pm 1\%$ wide at half maximum height, for a uniform spectrometer response $\pm 3\%$ wide, and for the radiative tail predicted by the Bethe-Heitler formula.

measurement,[17] was used as the primary monitor of the spectrometer momentum setting; but field reversibility was also tested directly with a Hall-effect probe. Although the efficiency of this probe differed for positive and negative fields by about 1%, this difference was measured and was found to be highly reproducible in independent tests with an NMR probe. When the appropriate correction was made, the Hall probe and shunt were reproducible to $\pm 0.1\%$ for the carefully Gaussed spectrometer, and the spectrometer field could be reversed to the same accuracy. The spectrometer momentum acceptance was $\Delta p/p \cong 6\%$.

The momentum of the elastically scattered particles differed from the incident momentum by less than 0.2% at all angles, this difference being due almost entirely to ionization in the target. Spectrum studies were made with the masks removed and with the spectrometer at 0° with respect to the measured beam direction. As in the measurements of beam direction, the transmitted particles were detected by the spectrometer ion chamber The results obtained for electrons and for positrons at 300 MeV are shown together in Fig. 2. The solid curve is the predicted spectrum for a trapezoidal incident-energy distribution $\pm 1\%$ wide at half maximum height, for a uniform spectrometer response $\pm 3\%$ wide, and for the radiative tail predicted by the Bethe-Heitler formula.[18] The trapezoidal incident distribution resulted from the finite size of the beam accepted by the collimator and from finite size of the beam spot at the target. The procedure just described is extremely fast; and since it has negligible statistical errors, it is rather more precise than the normal procedure in which counters are used in momentum analyzing the scattered particles.[19]

[17] J. Dupin, Doctoral dissertation.

[18] In calculations involving the Bethe-Heitler formula we have used the program described by R. A. Alvarez, Jr., HEPL-228, Internal Memorandum, 1961 (unpublished). This program is based on the article of H. W. Koch and J. W. Motz, Rev. Mod. Phys. 31, 920 (1959) and is expected to be accurate to about $\pm 2\%$.

[19] By using spectrometer ion chambers with high gain (a gain of several thousands being easily obtainable with manageable thicknesses of argon at one atmosphere pressure) and with typical electron intensities of greater than 1 μA, one can study various processes with high statistical precision over a range of cross sections greater than that covered in the present experiment. The method would be particularly useful in making absolute cross-section measurements at low momentum transfers and in systematically and precisely determining rms nuclear radii. In addition to the statistical advantages, one does not need to know the absolute efficiencies of the beam monitors, counters, or electronics, but only the relative efficiency of two "beam monitors," a quantity easily measured with the spectrometer at 0°. An "ion chamber ladder" could be constructed by splitting the collector plate into thin strips.

The scattered particles were detected in a two-counter telescope located at the focus of the spectrometer. A third counter, smaller than the telescope counters, was used to verify that the transmitted particles were well within the sensitive region of the telescope. The counters were well shielded, conservatively operated, and no trouble was observed from backgrounds or noise. Typical counting ratios were: doubles/singles=0.99, triples/doubles=1.00. The data obtained from the two-fold coincidence were recorded by scalers with resolving times of 20, 50, and 100 nsec as well as by scalers with resolving times greater than the beam pulse width. The beam pulse width was monitored during the experiment and was typically 500 nsec wide. Dead-time corrections were 1% or less, and the agreement among the different scalers indicated that this correction could be made to about 30% accuracy corresponding to an uncertainty of 0.3% or less in the counting rates.

III. DATA, CORRECTIONS, AND UNCERTAINTIES

With few exceptions, we have analyzed the present data and re-analyzed the previous high- and low-resolution data of Ref. 2 in the manner described in that reference. A more complete description of this analysis, as well as of the procedures used in obtaining data, is given in Ref. 7. The present changes are related to the multiple scattering problem mentioned in the Introduction and to the fact that different points in the three experiments have been measured with different angular resolutions. In order to permit a meaningful comparison of the measurements with one another and with theory, we have "unfolded" the effects of angular resolution, including multiple scattering, to obtain relative cross sections and electron-positron ratios in terms of their common denominator—the ideal case in which there is no multiple scattering and in which the geometrical angular resolution is perfect.

If parallel beams are assumed, three factors contribute to the experimental angular resolution: the finite beam size, multiple scattering, and the finite size of the spectrometer mask. Because the cross section is not a linear function of the scattering angle, the finite angular resolution affects the observed counting rates. While the variation of the *point* cross sections with angle is rapid only at small angles, the angular variation of *finite* nuclear cross sections such as cobalt and bismuth is dominated by the form factors for angles greater than about 10° or 20° at the present energies. Near the zeros of the Born approximation, the angular variation of the finite cross sections can be more rapid at large angles, e.g., even at angles greater than 100°, than at small angles.[3] Obviously, the factors which lead to errors in the scattering angle, as well as those which influence the angular resolution (including multiple scattering), can be just as important at large angles as at small angles. The effect can be quite different for positrons and electrons at the same angle or for relative positron or electron cross sections measured at neighboring points. While the result is generally to increase the measured cross section, the correction can change sign near the diffraction minimum, and it can be of opposite sign for positrons and electrons at the same angles. The failure to understand this point in Ref. 2 repeatedly frustrated attempts to reconcile, via multiple scattering, the discrepancies which occurred at both large and small angle points.

When the previous high-resolution and low-resolution experiments were compared with theory, the data were corrected in Ref. 2 for multiple scattering, while the geometrical contributions to the angular resolution were handled in Ref. 3 by folding together the theoretical partial-wave calculations with a Gaussian distribution having a standard deviation of 1°. The separation of the two processes is justified when the corrections are small; and the Gaussian approximation, while crude, does give a reasonable indication of the effects of the finite geometrical resolution.

The multiple scattering corrections of Ref. 2 were made by folding together the theoretical *point* cross sections with a Gaussian multiple scattering distribution. In the case of the low-resolution experiment, in which the ion chambers were upstream from the target, the target thickness for multiple scattering was taken to be the sum of the thicknesses in radiation lengths for the target and for the material upstream. The use of point cross sections in analyzing both experiments and the simple addition of multiple-scattering thicknesses in the low-resolution experiment greatly underestimated the effects of multiple scattering.

In the present analysis, the multiple scattering and beam spot distributions were first folded together at the center of gravity of the material upstream from the target and were then translated in three dimensions to the target, where the addition folds over multiple scattering, the unfolded cross sections, and the spectrometer mask were made. The multiple scattering theory of Nigam[20] was used, while the unfolded cross sections were obtained from the Yukawa model in the second Born-approximation[5] at the small angle points and from local fits to the results of the partial-wave calculations at the larger angles.

Since the physics of the problem tends to be obscured by the 8-fold numerical integration just described, we have used an approximate, two-dimensional analysis as a check. This second calculation used a Gaussian multiple-scattering distribution and the same unfolded cross sections as the three-dimensional analysis. For multiple scattering in the plane of the single scattering θ'_{ms}, the effective multiple-scattering angle for the material upstream from the target is related to θ_{ms}, the physical multiple scattering angle, by the equation

$$\theta_{\mathrm{ms}}'=\theta_{\mathrm{ms}}[1+(S_u/S_d)\cos\theta], \qquad (1)$$

where S_u is the distance between the target and the

[20] B. F. Nigam, Phys. Rev. **131**, 238 (1963).

origin of the multiple scattering, S_d is the distance between the target and the entrance mask of the spectrometer, and θ is the nominal single scattering angle determined by the spectrometer and by the incident-beam direction. Since the rms multiple-scattering angle is proportional to the square root of the thickness of material in radiation lengths, the effective thickness for the material upstream is proportional to the *square* of the quantity in brackets in Eq. (1). The enhancement $(\theta'_{\rm ms}/\theta_{\rm ms})^2$ at $\theta=0°$ is a factor of 5.3 in the previous experiment and a factor of 2.4 in the present experiment, where we have reduced S_u to the minimum distance consistent with a negligible "empty target" background. For the present experiment and for the previous low-resolution experiments, the thicknesses of material upstream of the target were 0.003 and 0.023 radiation lengths, respectively, while the total effective thicknesses were in the ratio of about $0.025/0.16\approx 1/6$.

The final correction for angular resolution was defined to be the difference between the assumed unfolded cross section and the folded cross section given by the three-dimensional calculation, divided by the folded cross section. The correction defined in this way is sensitive only to the angular variation of the assumed cross section in the region of interest and does not depend upon the normalization used. An error of 15% of the net correction was assigned to the relative cross-section measurements, while a minimum error of 1.5% was used when this was larger than the computed error. The latter is the estimated numerical precision of the three-dimensional calculation. The same multiple-scattering error was propagated into the electron-positron ratio defined by

$$R=(\sigma_--\sigma_+)/(\sigma_-+\sigma_+)\,, \qquad (2)$$

where σ_- and σ_+ are the differential cross sections for electrons and positrons. Results of the two multiple-scattering calculations were consistent within these errors and for cobalt as well as bismuth, there was at least one point where both the small-angle Born cross sections and the larger-angle partial-wave cross sections were expected to give reasonable results. At these points, the corrections agreed within the assigned errors.

Because point cross sections were used in assigning angle errors to the ratios given in Ref. 2, we have recomputed these errors. The assumed angular uncertainties for the relative (and absolute) cross sections were: $\pm 0.05°$, $\pm 0.2°$, and $\pm 0.01°$ for the previous low- and high-resolution experiments and for the present low-resolution experiment, respectively. The scattering angles were reproducible for positrons and electrons to $\pm 0.005°$, $\pm 0.03°$, and $\pm 0.01°$, respectively. In the high-resolution experiment, the beam direction was measured by exposing two x-ray negatives simultaneously at different locations along the beam line, a procedure which leads to somewhat larger errors than angle-cycling. The angular errors for the ratios were taken to be the square root of the sum of the squares of the errors in R assuming: (1) that positron and electron angles differed by the estimated angular reproducibility, and (2) that the data were taken at the same angle, but at an angle differing from the nominal scattering angle by the absolute angular uncertainty.

Although the "natural" angular acceptance of the spectrometer was expected to be much larger than either the 5-mm or the 20-mm mask, the acceptance measured in the scattering plane during the 300-MeV run was only slightly larger than the sum of the beam spot-width and the large mask diameter. Later it was discovered that an internal mask, located near the momentum slits, had not been removed. This mask reduced the width of the acceptance by about a factor of 2 and resulted in the anomalous width that was observed. The normalization of the large and small masks at the 15°, 300-MeV point indicated that the ratio of the cross sections with large over small mask was $(8.4\pm 2.2)\%$ smaller than would be predicted from the geometry. From the known spot width, mask width, and spectrometer width, we have calculated that losses of this magnitude would not occur unless the beam spot was at least 4 mm off the spectrometer axis. We consider such a misalignment to be improbable, in view of the ± 1 mm precision of the beam position indicator and the initial alignment accuracy. Furthermore, the averages of the electron and positron form factors at the corresponding 150- and 300-MeV points agree within their absolute errors (excluding the mask normalization error) when the large mask normalization is assumed. We have therefore used the large mask normalization and have assigned the normalization error to the relative cross sections at the 6° and 10°, 300-MeV points. A systematic mask error of $\pm 2\%$ has been assigned to the 15° and 20°, 300-MeV points to allow for a beam misalignment of $\pm$ 1mm. The absolute mask normalization error was taken to be $\pm 8.4\%$. The discrepancy between the large and small masks remains unexplained.

In the previous low-resolution experiment, an adjustable mask was used with a 3 mm width and a 6 mm height at the 10° cobalt point and at the 5°, 10°, and 15° bismuth points. A setting of 25 mm$\times$37 mm was used at the remaining points. A 50 mm $\times$ 37 mm mask was used in the high-resolution experiment, except at the normalization point where electron scattering on cobalt was measured with a 6 mm $\times$ 12 mm mask at 30°. The mask normalizations at the 20° points for both cobalt and bismuth in the low-resolution experiment indicated that the large mask was not completely contained within the solid angle of the spectrometer and that the actual solid angle was defined by the overlap of the two. This must also have been true for the large mask in the high-resolution experiment. We have used the small mask normalization in obtaining the relative cross sections for the low-resolution experiment, and we have normalized the high-resolution data for both cobalt and bismuth to the absolute cobalt point at 30°. Thus, the high- and low-resolution experiments are absolute with

independent normalization. We are unable, however, to assign systematic errors for the possible variation of the solid angle with spot position in the two previous experiments. Again, because the beam positions were continuously monitored and accurately reproduced for electrons and positrons, we anticipate that these errors would be about 2%.

Energy errors for the absolute cross sections were computed from the variation of the finite cross sections with energy and from the estimated energy uncertainties. The energies, determined independently in each case by the beam analyzing magnets and by the spectrometers, were (302±2)MeV for the previous low-resolution experiment (302±1)MeV for the previous high-resolution experiment, and (299±1) MeV and (149±1) MeV for the present measurements. While the variation of the cross sections for a given change in energy depends upon the point in question, the variations at different points are correlated. Thus, the energy errors for the relative cross sections and for the ratios are smaller than for the absolute cross sections.

The bremsstrahlung correction was calculated using the Bethe-Heitler[18] theory and contains the corrections for radiation before and after scattering. The virtual radiative corrections were calculated using the results of Tsai.[21] The small annihilation correction includes annihilation in the target, as well as in the scintillation counters and the spectrometer ion chamber.

Inelastic scattering was not expected to contribute significantly to the counting rates at the small angle points. At the larger angles, the inelastic scattering was measured for both positrons and electrons in the previous high-resolution experiment. Although we have used these results directly in the present analysis, the corrections and errors in the ratios are in some cases significantly different. Since the inelastic scattering is roughly equal for positrons and electrons, while the elastic scattering can be quite different, the correction to the ratio depends upon the value of the ratio after the other corrections have been made.

In the tables which follow, we have summarized the data and the principal corrections and uncertainties for the three experiments (see Tables I—III). In addition to the ratios, the analysis is given for the relative electron and positron cross-sections, none of which have been published previously. For the sake of brevity, the "uncorrected" values for σ_0 already contain corrections (δ) and errors (ϵ) for counting-rate losses and empty target background. A distinction has been made among relative errors ($\epsilon_{\rm rel}$), absolute errors ($\epsilon_{\rm abs}$), and the error in the electron or positron cross section which is propagated into the ratio. Except for ϵ_R, the final error in R, the various corrections and errors are given in percent. Small or constant corrections and errors are mentioned in the table headings. The inelastic contamination (f) from Ref. 2 is given for each point; but again for brevity, the inelastically corrected ratios and cross sections with appropriate errors have not been explicitly shown.

When the data are compared with theory, the results for a given experiment and element may be separately normalized, i.e., all points may be shifted by a constant factor. The final errors are then the relative errors (including the uncertainty in f) combined with the uncertainty in the normalization. These errors are of order 3%; thus they are smaller than the true absolute errors.

In Ref. 7, a normalization procedure is described in which the averages of the squares of the corrected form factors for positrons and electrons at the small angle points are fitted by a "model-independent" function based on the first Born approximation:

$$F^2(q^2)=\exp\,(-\tfrac{1}{3}q^2\langle r\rangle^2)\,, \tag{3}$$

where q is the four-momentum transfer, and $\langle r\rangle$ represents the rms radius of the nuclear charge distribution. The parameter $\langle r\rangle$ and the errors in this quantity are obtained from the relative cross-section data, while the normalization is found by requiring that $F^2(0)=1$. The use of the average of positron and electron form factors squared results in an approximate cancellation of the second term of the Born approximation, thus extending the range of validity of Eq. (3). The 10°, 20°, and 30° cobalt and the 5°, 10°, and 15° bismuth points were used in the normalization at 300 MeV; and the three corresponding bismuth points were used at 150 MeV. The cobalt and bismuth data from the previous high- and low-resolution experiments agree quite well at their common 30° points after the inelastic-scattering correction has been made; thus we have used the low-resolution normalization for both.

The results are summarized below. The error shown with $F^2(0)$ is the uncertainty in the normalization and should not be confused with the absolute errors in the data tables. The error shown with $\langle r\rangle$ is the uncertainty in this parameter if one assumes Eq. (3). A partial-wave analysis of the data would presumably lead to errors in $\langle r\rangle$ of the same order of magnitude, but the values themselves could change by more than the errors shown here. We therefore view Eq. (3) as being simply a convenient way of discussing the data in the absence of a partial-wave analysis.

Z	Experiment	$F^2(0)\pm\epsilon_{F^2}$	$(\langle r\rangle\pm\epsilon_{\langle r\rangle})$ (F)
Co^{59}	Stanford, 300 MeV	0.881±0.031	4.01±0.04
Bi^{209}	Stanford, 300 MeV	0.938±0.037	5.25±0.10
Bi^{209}	Orsay, 300 MeV	1.151±0.023	5.12±0.07
Bi^{209}	Orsay, 150 MeV	1.070±0.019	5.18±0.09
Bi^{209}	combined data	···	5.17±0.05

The rms radii determined from previous electron scattering experiments[4,22] are 3.83 F for cobalt and 5.52 F for bismuth with estimated uncertainties of about ±2%.

[21] Yung-Su Tsai, Phys. Rev. **122**, 1898 (1961).

[22] H. Crannell, R. Helm, H. Kendall, J. Oeser, and M. Yearian, Phys. Rev. **121**, 283 (1961).

TABLE I. Stanford low-resolution data. Column 4 gives the cross section after the counting rate and the background corrections have been made. Errors in these corrections are included in the statistical errors in column 15. The bremsstrahlung and the Schwinger radiative correction are given in columns 5 and 6, and the correction for angular resolution including multiple scattering appears in column 7. The miscellaneous corrections take into account the slight differences in energy and in the effective scattering angle as well as the effects of incorrect settings of the recoil spectrum, of beam monitoring, and of annihilation. The net correction, defined by $(1+\delta_{\text{net}})=\pi_i(1+\delta_i)$, is given in column 9. Energy and angle errors for the electron-positron ratios are given in columns 10 and 12, and for the relative cross sections in columns 11 and 13. The multiple-scattering error appears in column 14. The ratio, uncorrected for inelastic scattering, is shown in column 16 and the final error in the ratio in column 17. The latter was found by combining quadratically the appropriate systematic and the statistical errors given in the table with a miscellaneous error of $\pm 0.6\%$ due to uncertainties in beam monitoring, in the setting on the spectrum, and in annihilation, bremsstrahlung, and radiation. The "ratio" errors associated with the cross sections were propagated through Eq. (2) to find the error in the ratio. The un-normalized cross sections with final relative and absolute errors are given in columns 18, 19, and 20. The final relative error was found by combining quadratically the appropriate systematic and the statistical errors given in the table with the miscellaneous relative error resulting from beam monitoring bremsstrahlung, radiation and the mask normalization. The relative error due to radiation was $\pm 0.6\%$, while the error due to bremsstrahlung was $\pm 0.5\%$, except at the 40° cobalt points where it was $\pm 3.9\%$ due to doubling the target thickness. The mask normalization error was $\pm 2.4\%$ for the 20°, 30°, and 45° bismuth points, $\pm 2.2\%$ for the 20°, 30°, and 40° cobalt points, and zero elsewhere. The absolute error contains an additional $\pm 7.5\%$ due to the absolute uncertainties in the mask size, bremsstrahlung, radiation, target thickness, and beam monitoring. The final entry, taken from Ref. 2, is the inelastic contamination at each point.

1 Target	2 Energy (MeV)	3 Angle	4 σ_0 (cm²/sr)	5 δ_B (%)	6 δ_S (%)	7 δ_{MS} (%)	8 δ_{misc} (%)	9 δ_{net} (%)	10 $\epsilon_{E\text{-}R}$ (%)	11 $\epsilon_{E\text{-rel}}$ (%)	12 $\epsilon_{\theta\text{-}R}$ (%)	13 $\epsilon_{\theta\text{-rel}}$ (%)	14 ϵ_{MS} (%)	15 ϵ_{stat} (%)	16 R_{e+i}	17 ϵ_R	18 σ_{e+i} (cm²/sr)	19 ϵ_{rel} (%)	20 ϵ_{abs} (%)	21 f (Ref. 2)
e^-+Bi^{209}	302±2	5°	9.99×10^{-23}	+19.4	+7.2	−42.0	−2.1	−17.1	±0.1	±1.2	±0.4	±4.4	±6.0	± 0.7	+0.007	±0.042	8.20×10^{-23}	± 7.5	±11	<0.002
e^++Bi^{209}	302±2	5°	9.59×10^{-23}	+19.4	+7.2	−42.0	+5.0	−14.7	±0.1	±1.2	±0.4	±4.4	±6.0	± 0.9			8.10×10^{-23}	± 7.5	±11	<0.002
e^-+Bi^{209}	302±2	10°	3.36×10^{-24}	+19.6	+8.7	−21.9	+0.6	+2.1	±0.1	±0.7	±0.3	±2.4	±3.3	± 0.7	+0.002	±0.024	3.43×10^{-24}	± 4.4	±8	<0.003
e^++Bi^{209}	302±2	10°	3.29×10^{-24}	+19.6	+8.7	−21.9	+2.6	+4.1	±0.1	±0.7	±0.3	±2.4	±3.3	± 0.7			3.42×10^{-24}	± 4.4	±8	<0.003
e^-+Bi^{209}	302±2	15°	2.51×10^{-25}	+19.8	+9.5	−16.0	−0.4	+9.7	±0.3	±0.2	±0.3	±1.8	±2.4	± 1.0	−0.024	±0.018	2.76×10^{-25}	± 3.6	±8	<0.006
e^++Bi^{209}	302±2	15°	2.55×10^{-25}	+19.8	+9.5	−15.0	+1.8	+13.5	±0.3	±0.2	±0.3	±1.7	±2.3	± 1.3			2.89×10^{-25}	± 3.4	±8	<0.006
e^-+Bi^{209}	302±2	20°	1.92×10^{-26}	+20.0	+10.0	−22.8	−1.0	+0.9	±0.5	±1.2	±0.5	±2.5	±3.4	± 0.5	−0.208	±0.024	1.94×10^{-26}	± 5.0	±9	<0.04
e^++Bi^{209}	302±2	20°	2.76×10^{-26}	+20.0	+10.0	−19.5	+0.6	+6.9	±0.5	±1.2	±0.5	±2.1	±2.9	± 0.7			2.94×10^{-26}	± 4.5	±9	<0.03
e^-+Bi^{209}	302±2	30°	8.82×10^{-28}	+20.8	+11.0	−8.5	−1.5	+20.7	±0.3	±0.5	±0.1	±0.9	±1.5	± 1.8	+0.044	±0.020	1.06×10^{-27}	± 3.6	±8	0.072 ±0.017
e^++Bi^{209}	302±2	30°	7.93×10^{-28}	+20.8	+10.8	−8.9	+0.5	+20.6	±0.3	±0.5	±0.1	±1.0	±1.5	± 2.8			9.71×10^{-28}	± 4.2	±8	0.072 ±0.018
e^-+Bi^{209}	302±2	45°	1.19×10^{-29}	+23.3	+12.0	−0.9	−1.2	+35.1	±0.7	±0.2	±1.2	±0.1	±1.5	±18	−0.32	±0.12	1.61×10^{-29}	±18	±19	0.31 ±0.07
e^++Bi^{209}	302±2	45°	2.83×10^{-29}	+23.3	+11.8	−18.7	+0.2	+12.4	±0.7	±0.2	±1.3	±2.0	±1.8	±15			3.17×10^{-29}	±15	±16	0.13 ±0.05
e^-+Co^{59}	302±2	10°	3.94×10^{-25}	+17.9	+8.7	−19.8	+0.0	+2.8	±0.2	±0.8	±0.2	±2.2	±3.0	± 1.0	+0.016	±0.016	4.05×10^{-25}	± 4.0	±8	<0.003
e^++Co^{59}	302±2	10°	3.81×10^{-25}	+17.9	+8.7	−19.7	+0.1	+2.9	±0.2	±0.8	±0.2	±2.2	±3.0	± 1.0			3.92×10^{-25}	± 4.0	±8	<0.003
e^-+Co^{59}	302±2	20°	8.16×10^{-27}	+18.2	+10.0	−14.6	+1.7	+12.9	±0.3	±0.4	±0.3	±1.6	±2.2	± 0.8	−0.034	±0.016	9.21×10^{-27}	± 3.7	±8	<0.035
e^++Co^{59}	302±2	20°	8.65×10^{-27}	+18.2	+10.0	−12.4	+0.1	+14.0	±0.3	±0.4	±0.3	±1.3	±1.9	± 0.8			9.85×10^{-27}	± 3.5	±8	<0.035
e^-+Co^{59}	302±2	30°	1.99×10^{-28}	+19.0	+11.0	−15.7	+3.0	+14.9	±0.3	±1.5	+0.2	±1.7	±2.4	± 0.7	−0.184	±0.020	2.28×10^{-28}	± 3.9	±8	0.17 ±0.04
e^++Co^{59}	302±2	30°	2.93×10^{-28}	+19.0	+10.8	−14.5	+0.1	+12.9	±0.3	±1.5	±0.2	±1.6	±2.2	± 1.2			3.31×10^{-28}	± 3.9	±8	0.12 ±0.03
e^-+Co^{59}	302±2	40°	5.0×10^{-30}	+51.0	+11.6	+0.9	+0.0	+69.9	±0.6	±3.8	±1.7	±0.1	±1.5	± 4.3	−0.15	±0.047	8.5×10^{-30}	± 7.5	±10	0.62 ±0.12
e^++Co^{59}	302±2	40°	8.9×10^{-30}	+51.0	+11.4	−23.0	+0.1	+29.7	±0.6	±3.8	±1.9	±2.5	±3.5	± 6.7			1.15×10^{-29}	± 9.7	±12	0.42 ±0.08

TABLE II. Stanford high-resolution experiment. The format used here is the same as in Table I. The miscellaneous errors were ±1.5% for the ratio, ±1.5% for the relative cross sections, and ±6.0% for the absolute cross sections. Since the data for cobalt and bismuth were taken during a single run in which only the target was changed between points and since the errors in target thickness were small, the appropriate errors when cobalt and bismuth points are compared are the relative errors, not the absolute errors as in Table I. All data were normalized to an absolute electron-cobalt measurement at 30° taken with a special small mask during the same run.

1 Target	2 Energy (MeV)	3 Angle	4 σ_0 (cm²/sr)	5 δ_B (%)	6 δ_S (%)	7 δ_{MS} (%)	8 δ_{misc} (%)	9 δ_{net} (%)	10 ϵ_{E-R} (%)	11 ϵ_{E-rel} (%)	12 $\epsilon_{\theta-R}$ (%)	13 $\epsilon_{\theta-rel}$ (%)	14 ϵ_{MS} (%)	15 ϵ_{stat} (%)	16 R_{e+i}	17 ϵ_R	18 σ_{e+i} (cm²/sr)	19 ϵ_{rel} (%)	20 ϵ_{abs} (%)	21 f (Ref. 2)
e^-+Bi^{209}	302±1	30°	6.80×10^{-28}	+35.8	+17.0	−4.0	0.0	+52	±1.5	±1.5	±0.7	± 3.6	±1.5	± 1.6	+0.051	±0.025	1.03×10^{-27}	± 4.7	± 7.7	0.03
e^++Bi^{209}	302±1	30°	6.15×10^{-28}	+35.8	+17.0	−4.4	+0.5	+52	±1.5	±1.5	±0.7	± 4.0	±1.5	± 2.3			9.32×10^{-28}	± 5.3	± 8.0	0.03
e^-+Bi^{209}	302±1	35°	1.12×10^{-28}	+36.4	+17.5	−8.1	0.0	+48	±1.5	±1.5	±2.9	± 7.2	±1.5	± 4.1	−0.177	±0.040	1.67×10^{-28}	± 8.6	±11	0.03
e^++Bi^{209}	302±1	35°	1.54×10^{-28}	+36.4	+17.5	−3.7	+0.5	+55	±1.5	±1.5	±2.8	± 3.9	±1.5	± 4.0			2.39×10^{-28}	± 6.3	± 8.7	0.02
e^-+Bi^{209}	302±1	40°	1.80×10^{-29}	+36.8	+18.0	−9.9	0.0	+46	±1.5	±1.5	±2.2	± 8.8	±1.5	± 8.6	−0.396	±0.097	2.62×10^{-28}	±13	±15	0.03
e^++Bi^{209}	302±1	40°	4.05×10^{-29}	+36.8	+18.0	−7.2	+0.5	+50	±1.5	±1.5	±1.7	± 6.4	±1.5	± 7.7			6.04×10^{-29}	±10	±12	0.01
e^-+Bi^{209}	302±1	45°	8.10×10^{-30}	+37.6	+18.3	−0.9	0.0	+62	±1.5	±1.5	±6.5	± 0.8	±1.5	±10	+0.020	±0.17	1.30×10^{-29}	±11	±13	0.05
e^++Bi^{209}	302±1	45°	8.70×10^{-30}	+37.6	+18.3	−11.8	+0.5	+44	±1.5	±1.5	±6.7	±10	±1.8	±15			1.25×10^{-29}	±18	±19	0.05
e^-+Co^{59}	302±1	30°	1.42×10^{-28}	+41.7	+17.0	−8.7	0.0	+52	±1.5	±1.5	±1.1	± 6.8	±1.5	± 2.3	−0.185	±0.028	2.20×10^{-28}	± 7.2	± 9.4	0.13
e^++Co^{59}	302±1	30°	2.09×10^{-28}	+41.7	+17.0	−9.3	+0.2	+50	±1.5	±1.5	±1.1	± 6.4	±1.5	± 2.6			3.20×10^{-28}	± 6.9	± 9.2	0.09
e^-+Co^{59}	302±1	35°	1.55×10^{-29}	+42.0	+17.5	−16.0	0.0	+40	±1.5	±1.5	±3.9	±11	±2.4	± 5.6	−0.343	±0.043	2.20×10^{-29}	±13	±14	0.19
e^++Co^{59}	302±1	35°	2.97×10^{-29}	+42.0	+17.5	−9.6	+0.2	+50	±1.5	±1.5	±3.6	± 6.4	±1.5	± 5.0			4.52×10^{-29}	± 8.2	±10	0.10
e^-+Co^{59}	302±1	40°	4.45×10^{-30}	+42.6	+18.0	+1.9	0.0	+71	±1.5	±1.5	±5.1	± 1.2	±1.5	± 9.7	+0.097	±0.102	7.75×10^{-30}	±10	±12	0.19
e^++Co^{59}	302±1	40°	4.23×10^{-30}	+42.6	+18.0	−12.3	+0.2	+49	±1.5	±1.5	±5.3	± 8.4	±1.8	±16			$6.39-10^{-30}$	±18	±19	0.20
e^-+Co^{59}	302±1	45°	3.40×10^{-30}	+43.4	+18.3	+2.0	0.0	+73	±1.5	±1.5	±0.9	± 1.4	±1.5	± 8.7	+0.207	±0.086	5.98×10^{-30}	± 9.2	±11	0.05
e^++Co^{59}	302±1	45°	2.18×10^{-30}	+43.4	+18.3	+0.2	+0.2	+70	±1.5	±1.5	±0.8	± 0.2	±1.5	±16			3.77×10^{-30}	±17	±18	0.08

TABLE III. Orsay low-resolution data. The format is again as in Table I. The miscellaneous errors were about ±2% for the ratios and relative cross sections at 300 MeV and ±0.4% at 150 MeV. The larger errors at 300 MeV result from the mask normalization described in the text. The miscellaneous absolute error of ±10% is dominated by the (8.4±2.2)% absolute discrepancy in the normalization of the large and small masks. We have chosen to use the large mask normalization since only the 6° and 10° points at 300 MeV were taken with the small mask and since the internal consistency of the 300- and 150-MeV data would be lost if the 300-MeV data were separately normalized with the small mask. We wish to emphasize that the mask discrepancy is much larger than our *a priori* estimates of the mask error and that we are assuming that the cause or causes of this discrepancy have not affected the relative cross section or ratio measurements.

1 Target	2 Energy (MeV)	3 Angle	4 σ_0 (cm²/sr)	5 δ_B (%)	6 δ_S (%)	7 δ_{MS} (%)	8 δ_{misc} (%)	9 δ_{net} (%)	10 ϵ_{E-R} (%)	11 ϵ_{E-rel} (%)	12 $\epsilon_{\theta-R}$ (%)	13 $\epsilon_{\theta-rel}$ (%)	14 ϵ_{MS} (%)	15 ϵ_{stat} (%)	16 R_{e+i}	17 ϵ_R	18 σ_{e+i} (cm²/sr)	19 ϵ_{rel} (%)	20 ϵ_{abs} (%)	21 f (Ref. 2)
e^-+Bi^{209}	299±1	6°	4.70×10^{-23}	+7.8	+7.5	−12.5	0.0	+1.4	±0.5	±0.5	±0.9	±0.9	±1.9	± 1.0	−0.004	±0.017	4.77×10^{-23}	± 3.2	±11	<0.002
e^++Bi^{209}	299±1	6°	4.73×10^{-23}	+7.8	+7.5	−12.5	+0.3	+1.7	±0.5	±0.5	±0.9	±0.9	±1.9	± 1.0			4.81×10^{-23}	± 3.2	±11	<0.002
e^-+Bi^{209}	299±1	10°	3.82×10^{-24}	+7.8	+8.9	−5.8	0.0	+10.6	±0.7	±0.7	±0.5	±0.5	±1.5	± 0.7	±0.014	±0.015	4.22×10^{-24}	± 2.9	±11	<0.003
e^++Bi^{209}	299±1	10°	3.70×10^{-24}	+7.8	+8.9	−5.8	+0.3	+10.9	±0.7	±0.7	±0.5	±0.5	±1.5	± 1.2			4.10×10^{-24}	± 3.1	±11	<0.003
e^-+Bi^{209}	299±1	15°	3.06×10^{-25}	+7.9	+9.7	−3.2	0.0	+14.6	±0.9	±0.9	±0.4	±0.4	±1.5	± 0.7	−0.068	±0.020	3.51×10^{-25}	± 2.8	±11	<0.006
e^++Bi^{209}	299±1	15°	3.49×10^{-25}	+7.9	+9.7	−2.8	+0.3	+15.3	±0.9	±0.9	±0.3	±0.3	±1.5	± 0.6			4.02×10^{-25}	± 2.8	±11	<0.006
e^-+Bi^{209}	299±1	20°	2.67×10^{-26}	+8.0	+10.3	−4.3	0.0	+14.0	±1.2	±1.2	±0.5	±0.5	±1.5	± 2.0	−0.168	±0.028	3.04×10^{-26}	± 3.5	±11	<0.04
e^++Bi^{209}	299±1	20°	3.72×10^{-26}	+8.0	+10.3	−3.8	+0.3	+14.8	±1.2	±1.2	±0.4	±0.4	±1.5	± 3.2			4.27×10^{-26}	± 4.3	±11	<0.03
e^-+Bi^{209}	149±1	10°	2.71×10^{-23}	+7.8	+7.8	−11.0	0.0	+3.4	±1.2	±1.2	±0.4	±0.4	±1.7	± 0.6	+0.085	±0.016	2.80×10^{-23}	± 2.2	±10	<0.002
e^++Bi^{209}	149±1	10°	2.27×10^{-23}	+7.8	+7.8	−11.2	−1.4	+4.1	±1.2	±1.2	±0.4	±0.4	±1.7	± 0.7			2.36×10^{-23}	± 2.2	±10	<0.002
e^-+Bi^{209}	149±1	20°	1.000×10^{-24}	+7.8	+9.3	−3.7	0.0	+13.4	±1.6	±1.6	±0.3	±0.3	±1.5	± 0.6	+0.043	±0.017	1.134×10^{-24}	± 2.3	±10	<0.003
e^++Bi^{209}	149±1	20°	9.10×10^{-25}	+7.8	+9.3	−3.3	−2.0	+14.3	±1.6	±1.6	±0.3	±0.3	±1.5	± 1.3			1.040×10^{-24}	± 2.6	±11	<0.003
e^-+Bi^{209}	149±1	30.3°	6.76×10^{-26}	+7.9	+10.1	−1.8	0.0	+16.7	±2.3	±2.3	±0.2	±0.2	±1.5	± 1.5	−0.097	±0.032	7.89×10^{-26}	± 3.1	±11	<0.006
e^++Bi^{209}	149±1	30.3°	8.14×10^{-26}	+7.9	+10.1	−1.2	−3.2	+17.8	±2.3	±2.3	±0.2	±0.2	±1.5	± 4.9			9.59×10^{-26}	± 5.7	±12	<0.006
e^-+Bi^{209}	149±1	40.35°	5.76×10^{-27}	+8.0	+10.7	−1.5	0.0	+17.8	±3.0	±3.0	±0.2	±0.2	±1.5	± 3.8	−0.265	±0.085	6.79×10^{-27}	± 5.0	±11	<0.04
e^++Bi^{209}	149±1	40.35°	9.88×10^{-27}	+8.0	+10.7	−1.5	−4.3	+18.3	±3.0	±3.0	±0.2	±0.2	±1.5	±16			1.17×10^{-28}	±16	±19	<0.03

DISCUSSION

The ratios obtained for cobalt and bismuth are shown corrected for inelastic scattering in Figs. 3 and 4. The curves labeled R_{point}, R_{Yukawa}, and R_{uniform} were calculated from the second Born formulas given by McKinley and Feshbach,[23] Lewis, and Drell and Pratt.[5] The curves labeled R_{HCR} are the results of the partial-wave calculations of Herman, Clark, and Ravenhall[3] based on the electron data of Ref. 4. The 150-MeV bismuth data have been scaled to 300 MeV using the second Born, small angle expression

$$R=Z\alpha G(q)/E, \tag{4}$$

where $G(q)$ depends only on the momentum transfer q, α is the fine-structure constant, and E is the incident energy.

Looking now at Fig. 3 (and comparing it with Fig. 6 in Ref. 2), we observe that the experimental discrepancy at the 40° point is about 2 standard deviations (it was over 3 standard deviations), while the difference between experiment and theory at the 45° point is now less than 1 standard deviation (it was about 2.5 standard deviations). The dominant errors at these points are statistical as before.

Turning now to the small-angle bismuth data in Fig. 4, we note that the agreement between experiment and theory at the 15° and 20° points is good, but could improve by *decreasing* the rms radius. This is consistent with the fact that the "rms radii" obtained by fitting the present bismuth data with Eq. (3) are smaller than the value reported in Ref. 4. The agreement between the 300-MeV data and the scaled 150-MeV data of the present experiment is excellent except at the points near 5°, which differ by 2.2 standard deviations. This confirms the previous result in which the 300-MeV data of Ref. 2 disagreed with the scaled data of Ref. 1 taken at energies below 170 MeV. Because of the large multiple scattering correction and associated error, the previous measurement at 5° is no longer very sensitive. It is worth noting, however, that the value has been changed very little by the corrections and that this value is within the error assigned for the present result. If one is willing to assume some cancellation of the multiple-scattering uncertainties in the ratio measurement instead of propagating an error equal to the relative

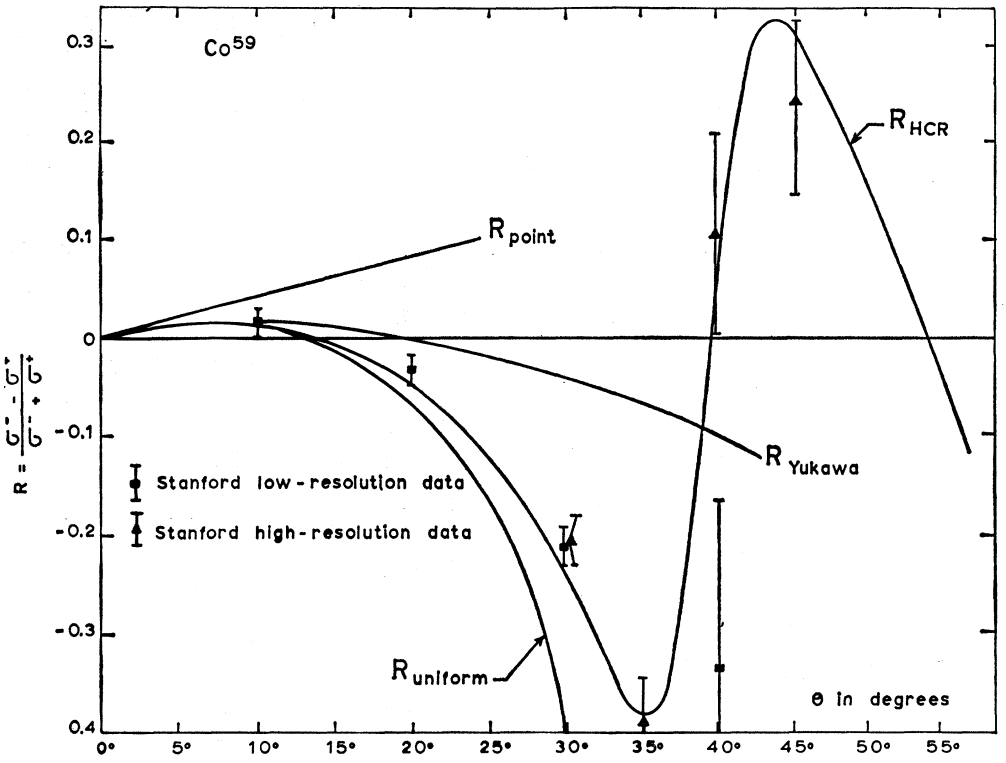

FIG. 3. The ratio R for Co^{59} at 302 MeV. The curves represent theoretical predictions for point, Yukawa, and uniform charge distributions calculated in the second Born approximation. The curve labeled R_{HCR} gives the phase-shift calculation of Herman, Clark, and Ravenhall for a sharp angular resolution.

[23] W. A. McKinley, Jr. and H. Feshbach, Phys. Rev. **74**, 1759 (1948).
[24] R. R. Lewis, Jr., Phys. Rev. **102**, 537 (1956).

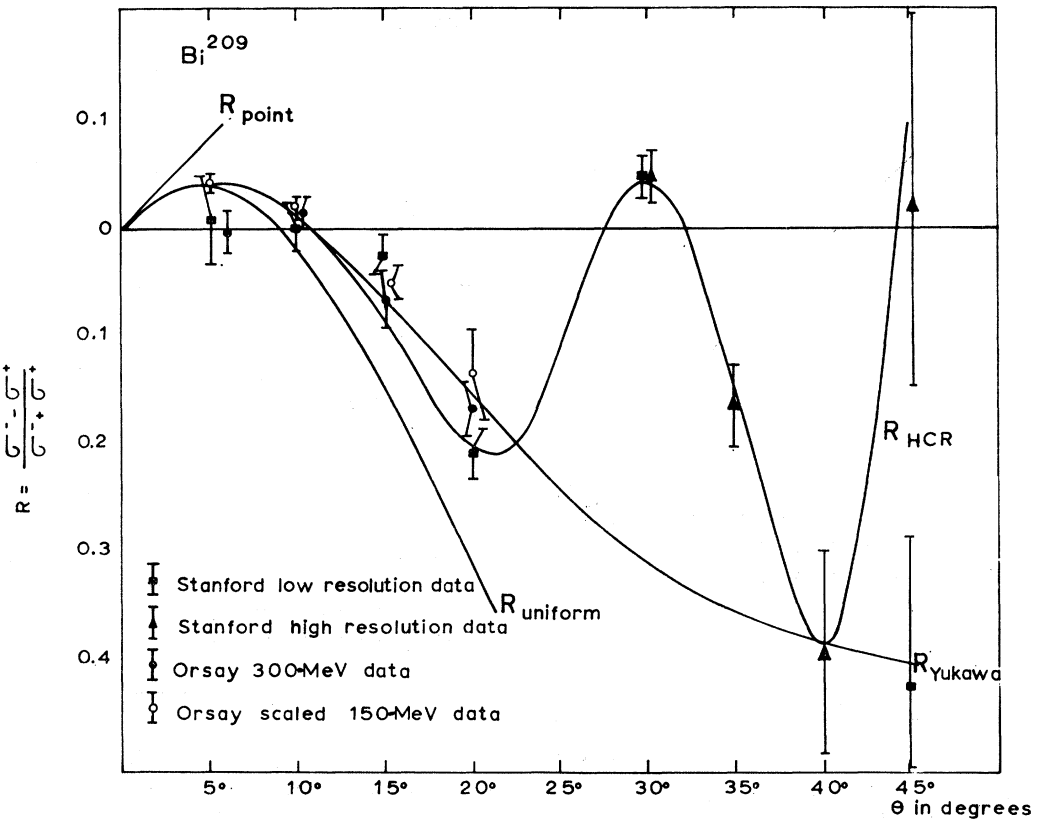

FIG. 4. The ratio R for Bi^{209} at 300 MeV. The solid curves are the theoretical predictions for point, Yukawa, and uniform charge distributions calculated in the second Born approximation. The curve labeled R_{HCR} gives the phase-shift calculation of Herman, Clark, and Ravenhall for a sharp angular resolution. The 150-MeV results of the present experiment have been scaled to 300 MeV using Eq. (4).

error, as we have done, the consistency of the two results and the apparent failure of the scaling law become more striking.

The squares of the "absolute" form factors for the normalized bismuth data at the four small-angle points are shown as a function of q^2 in Fig. 5. Also shown is the fit obtained from Eq. (3) for the combined data at the three smallest angles. The fit to the exponential is good at these angles but appears to be deteriorating at the 20° points. The internal consistency of the normalized data is excellent; and the energy-dependent differences in the electron and positron form factors predicted by Eq. (4) are clearly demonstrated by the greater separation of the 150-MeV positron and electron points.

The squares of the "absolute" electron and positron form factors for all of the normalized cobalt and bismuth cross sections are shown as a function of q^2 in Fig. 6. Also shown are the 183-MeV electron data of Ref. 4. from which the partial-wave results were derived, as well as the more recent 183-MeV data of Crannel *et al.*[22] The over-all accuracy of the former was "of the order of ±10%", while the latter were "reproducible to no better than 10% for repeated runs at the same target and target angle when the statistical errors were of order 2–3%." The solid curves for electrons and positrons were derived from the second Born approximation at small q^2 and from the partial-wave calculations[3] at larger momentum transfers. Since, as we have already noted, the form factors are not simply a function of q^2, the comparison of form factors obtained at different energies must be viewed with caution. The agreement between the previous high- and low-resolution experiments is now seen be to excellent except at the 40° electron points for cobalt and at the 45° positron points for bismuth. The experimental discrepancies which still exist in the ratios can be associated directly with these points. Since the same normalization factors were used for the two Stanford experiments, the absolute agreement for both cobalt and bismuth at the other points under quite different experimental conditions is significant.

The uncertainties in the relative and absolute cross sections reported here are generally smaller than those estimated for the electron scattering experiments of Refs. 4 and 22. At the same time, the positron data extend over a range of q^2 greater than that covered by the electron measurements. We have reason to hope, therefore, that a more precise determination of the

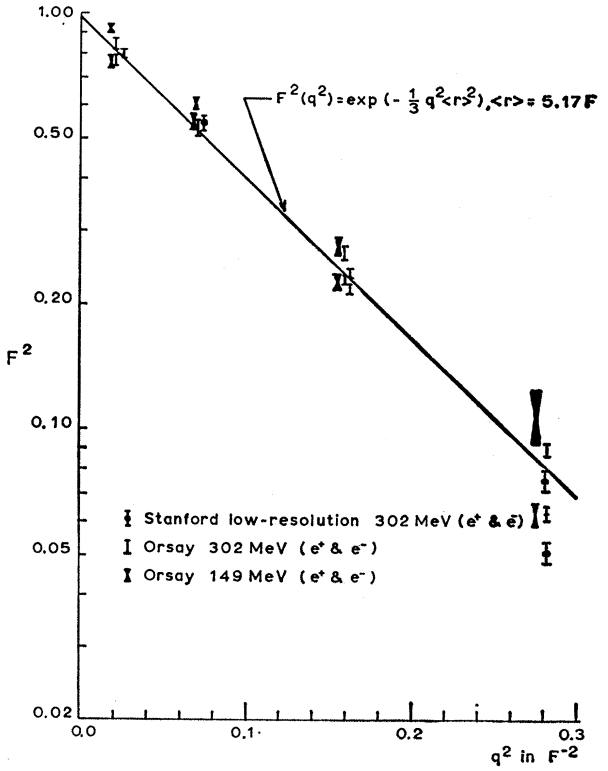

FIG. 5. Bismuth form factors at the small-angle points. The Orsay and Stanford data have been normalized separately via Eq. (3) with $\langle r\rangle=5.17$ F. This appears in the figure as a straight line passing through $F^2(0)=1$. The errors are the net relative errors of Tables I and II.

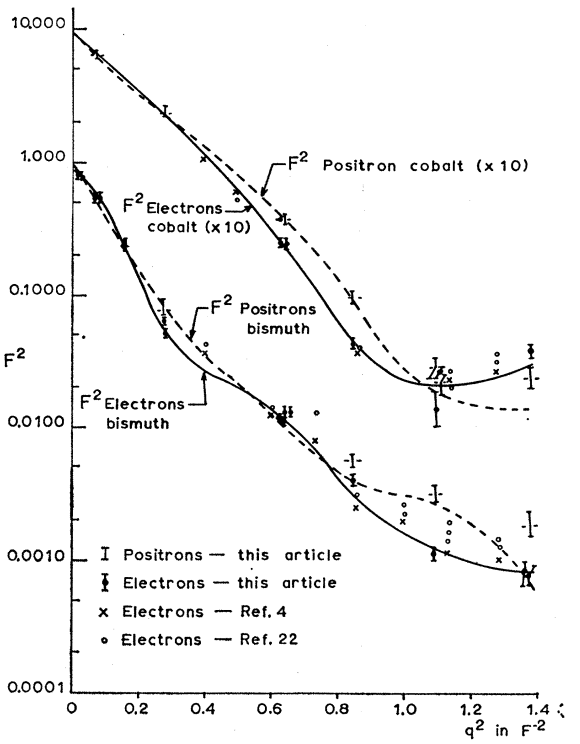

FIG. 6. Bismuth and cobalt form factors as a function of q^2. (Those for cobalt were multiplied by 10 before plotting.) The solid curves for electrons and positrons were derived from the second Born approximation at small q^2 and from the partial-wave calculations of Herman, Clark, and Ravenhall at the larger momentum transfers. The Orsay and Stanford data have been separately normalized via Eq. (3), but the same normalization was used for the Stanford high- and low-resolution experiments for each element. Also shown are the 183-MeV electron data of Ref. 4 from which the partial-wave results were derived, as well as the more recent 183-MeV data of Ref. 22. The presentation of the form factors as a function of q^2 (approximately $\propto\theta^2$) permits an *approximate* comparison of data taken at different energies, but obscures an important experimental consideration, namely that the variation of the cross sections with angle can be just as rapid at large angles as at small angles.

charge distribution parameters for cobalt and bismuth will now be possible. It would be interesting to see whether a partial-wave fitting of the combined electron and positron data will lead to values for the nuclear charge parameters which are significantly more precise than those determined from the electron data alone. Finally the disagreement between the ratios measured near 5° at 300 MeV on bismuth and those measured at lower energies and scaled to 300 MeV remains to be explained.

ACKNOWLEDGMENTS

We are expecially indebted to Professor J. Goldemberg for his participation in the design of the experiment and for many helpful discussions throughout the course of this work. We are also grateful to Professor Goldemberg and to Professor J. Pine for reading this manuscript before it was submitted for publication.

Dr. Burnod developed and adapted the Orsay positron beam to suit our needs. R. Tchapoutian participated in the data runs. In addition, we would like to acknowledge the support of Professor Blanc-Lapierre and Dr. B. Milman as well as the generous help of the linear accelerator personnel. One of us (DY) was supported by a National Science Foundation Postdoctoral Fellowship during the course of this work.